Charge-exchange-excited line radiation in a tokamak (ASDEX) with neutral-particle-beam injection

P. G. Carolan, B. P. Duval,* A. R. Field,† S. J. Fielding, N. C. Hawkes, and N. J. Peacock
EURATOM—United Kingdom Atomic Energy Authority Fusion Association, Culham Laboratory, Abingdon-Oxon, OX14 3DB, United Kingdom

G. Fussmann, G. Janeschitz, and J. Hofmann
Max-Planck-Institute für Plasmaphysik—EURATOM Association, D-8046 Garching, Germany

K. H. Behringer
JET Joint Undertaking, Abingdon-Oxon, OX14 3EA, United Kingdom

R. C. Isler
Fusion Energy Division, Oak Ridge National Laboratory, Oak Ridge, Tennessee 37830
(Received 23 June 1986)

Time sequences of the spectral emission from the ASDEX tokamak at the Max-Planck-Institute für Plasmaphysik have been recorded using multichannel survey spectrometers operating over the wavelength range 100—7000 Å. During injection of neutral beams of hydrogen or deuterium, charge-exchange- (CX) excited lines, mostly $\Delta n = 1,2$ transitions from hydrogenic ions of intrinsic impurity elements or injected trace gases, are prominent throughout this entire spectral region. The charge-exchange origin of the lines is established by the temporal and spatial dependence on the injected beam current and also, in the case of visible transitions, by their relatively large spectral widths. With a beam power of 1.7 MW and an extraction potential of 41.5 keV, excitation of intrinsic impurity ions, e.g., O^{7+} ($n < 11$) and C^{5+} ($n < 9$) occurs routinely while, depending on the plasma conditions, other trace impurities, for example, F^{8+} ($n = 9$), Cl^{16+} ($n = 13$), S^{13+} ($n \leq 15$), and Kr^{25+} ($n \leq 22$) are also observed. From the absolute intensities of the C^{5+} and O^{7+} CX lines, impurity concentrations are deduced. Comparison of the concentration data derived from the vacuum-ultraviolet and separately from the visible intensities allows an assessment of the theoretical cross sections for charge-transfer recombination into different quantum states. Spectral line profiles of the CX transitions in the visible region involving high-n Rydberg states are consistent with bulk plasma and ion thermal motion. Coincidence between Rydberg levels of different ions with the same effective nuclear charge offers a plausible explanation for the appearance of some visible CX lines in the absence of atomic beams.

I. INTRODUCTION

Since the recognition that charge-transfer reactions between neutral hydrogen and ionized impurities[1,2] provide a unique method for measuring the concentrations of impurity nuclei, the use of charge-exchange recombination (CXR) spectroscopy as a diagnostic technique in high-temperature (particularly tokamak) plasmas has become widespread. Often, in the past, the diagnostic use of CX excitation resulting from H^0 or D^0 injection has been parasitic to the main function of the neutral beams, i.e., plasma heating. Custom-built neutral beams, however, have been developed which, when dedicated to the CX-excitation diagnostic, allow spatially resolved measurements of the plasma parameters.[3] The volume emissivities of the CX-excited lines depend on the product of the local neutral-particle density and the impurity concentration in the plasma. Provided, therefore, that the attenuation of the energy fractions in the beam is modeled correctly[4] and that the effective excitation rates following CXR are known and contribute a measurable amount to the line intensity, then from these data the impurity concentrations, even of bare nuclei, can be derived. At impact velocities of the order of an atomic unit (2.2×10^8 cm s^{-1}), the effective cross sections for CX excitation are considered to be theoretically well established, at least for the case of hydrogenic ions involving $n \sim m$, where m is the principal quantum shell of the recombined ion into which direct transfer recombination has a maximum probability. For hydrogenic ions, the bulk of the states populated by charge-exchange collisions decay promptly via a cascade of $\Delta n = 1,2$ transitions between states of maximum angular momentum—the so-called "yrast" transitions. These transition intensities have been used to measure the absolute sensitivity of tokamak-viewing, vacuum-ultraviolet (vuv) spectrometers.[5] This calibration technique has a particular appeal in the present experiments on the axi-symmetric-divertor-experiment (ASDEX) where both tokamak vuv- and visible-range spectrometers viewing the neutral-beam-heated tokamak employ multi-spectral channel detectors. An extended series of yrast transitions involving principal quantum levels from $n = 2$ to 10, or higher, can, in principle, be recorded simultaneously.

One aim in the present charge-exchange experiments, which were carried out during the ASDEX tokamak neutral-beam-heating program,[6] has been to survey the spectrum for CX-excited lines, a task not undertaken extensively in previous CX studies. An attempt is made to relate the observed yrast intensities to the theoretical CX cross sections.[7,8] An additional objective has been to establish what fraction of the line intensities, which are commonly observed to be enhanced during beam injection, is attributable to direct charge transfer from the neutral beam and not to concomitant changes in the ionization balance or cross-field impurity transport with subsequent electron-impact excitation of the recombined ion.[9] In typical tokamak conditions this alternative excitation will occur on a time scale $\gtrsim 1$ ms, i.e., the characteristic time for relaxation of the ionization balance due to electron impact, whereas yrast decay resulting from CX will follow the neutral-beam current time history on a much faster time scale. Previous CX studies particularly of the high-quantum-state transitions in the visible region have tended to rely, *per se,* on approximate wavelength coincidences with the charge-transfer line and their intensity enhancement during beam injection as corroboration of the CX process. Appreciable yrast line intensity prior to and following beam injection and even observations of intensity outside the beam irradiation volume[10] have complicated the simple picture of beam-induced CX. We have attempted to differentiate the beam-induced CX process from other excitation mechanisms by spatial measurements and by supplementing the slow multichannel readout detectors with fast-response photomultipliers capable of following beam switchoff on a submillisecond time scale. We concentrate our discussion on those lines which have been unambiguously identified as CX lines arising from atomic-beam-heating conditions in the ASDEX tokamak in the spectral region 100—7000 Å.

The spectral profiles of the visible yrast lines yield further information on ion temperature[11,12] and bulk plasma rotation.[13,14] In the visible region we find that identification of the CX lines is assisted greatly by the contrast between their large spectral widths and the relatively narrow background lines which are typical of edge plasma emission. Once the CX character of the lines is established, the diagnostic information on ion temperature and rotation is readily extracted and the values are wholly consistent with that expected from the tokamak performance.

The absolute intensities of the CX lines depend not only on the direct-charge-transfer (n,l) cross sections but also on possible redistribution of the quantum states due to plasma fields and particle collisions.[15] This problem becomes quite complex for $n > m$, see, e.g., Janev.[16] As a working relation,

$$m = z^{0.77} ,$$

where z is the ionic charge. The cross section for charge-transfer recombination directly into levels above m' is sensitive to the beam energy and with this in mind the neutral-beam energy fractions from the ASDEX injectors have been measured. Various cascade models for calculating the effective cross section for CX excitation of the observed lines are considered.

II. EXPERIMENTAL ARRANGEMENT

The ASDEX tokamak at the Max Planck Institut für Plasmaphysik has several different heating methods which are currently being studied. The impurity behavior during Ohmic-heating discharges, with additional neutral-beam injection (NBI) heating, ion cyclotron-resonance heating (ICRH), or lower hybrid wave heating (LHWH), has been described by Fussmann *et al.*[17]

Pertinent to the present paper on charge-exchange spectroscopy is the arrangement for neutral-beam injection heating. Two beam lines, each capable of delivering 1.75 MW of H^0 atoms or 2.1 MW of D^0 atoms at a beam energy of 41.5 keV, irradiate the plasma at an angle of 30° to the minor torus axis. The current for each beam line is fed from four sources, pairs of which can be switched independently. The rise time to reach full beam current is ~ 20 ms typically, whereas the cutoff times of the beam sources are relatively abrupt, $\sim 50\ \mu$s.

The dispositions of the beam-viewing spectrometers and the beam geometry are shown in Fig. 1. Two viewing line of sights were adopted, each incidentally intersecting the axis of the neutral beam in the outside half of the minor plasma diameter. Viewing position *A*, which was immediately "downstream" of the injection port, intersected the beam axis at an angle of 48° and at a location 19 cm from the minor torus axis. Viewing position *B*, the "upstream" viewing position, intersected the beam nearly normally, at an angle of 80° and at a location 28 cm outside of the minor axis. Apart from these differences in the plasma radii, both viewing lines admitted light from nearly the same volume and the same irradiated plasma conditions, the beam attenuation at this azimuthal position being only about 20%. The downstream viewing position *A* was occupied either by a vuv-range spectrometer, Model No. 251 from Schoeffel McPherson Instrument Co., which with the choice of either of two gratings could operate from 100 to 1700 Å, or a visible-range spectrometer which covered the wavelength region 2200—7000 Å. The upstream viewing position was occupied by a similar visible-range spectrometer. All the spectrometers were equipped with optical multichannel detector systems (OMA's) with identical recording and control electronics. The visible-range instruments had the additional option of photomultipliers for faster-time-resolved measurements.

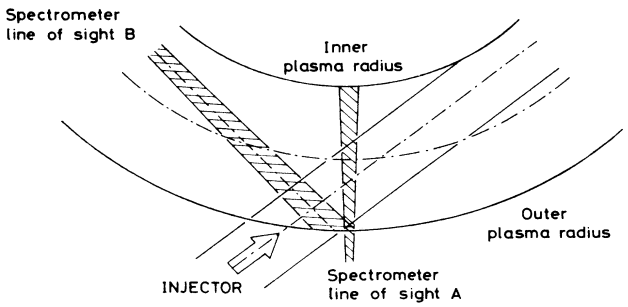

FIG. 1. Geometry of SE beam on ASDEX with hatched areas representing the plasma viewed by the spectrometers.

Light fibers were used to transmit data from the spectrometers attached to the torus and a remote, stand-alone data-acquisition system (SADA), and to send commands in the reverse direction, allowing exploitation of the various flexible readout modes of which the OMA's are capable. Generally, all 1024 OMA channels were read out in a period of 16 ms. In this "survey mode," 16 ms represents the minimum time resolution and up to 128 frames could be recorded during one discharge. The usual practice was followed of taking a spectral scan before plasma initiation which was then used to subtract ambient light and a "fixed" pattern of noise from the subsequent time frames. The 16-ms time frame of the survey mode is not sufficiently short to demonstrate the characteristic fast time response of the charge-exchange-excited lines, whose intensities should follow the neutral-beam current. For this purpose it was necessary to operate the OMA like a polychromator, by reading out in time the spectrally integrated information from a limited number of pixel groups. In this polychromator mode it was possible to achieve a time resolution of ~ 1 ms. A still shorter time resolution (<0.1 ms) was achieved with the visible-range instruments when operated with photomultiplier detectors.

The vuv survey spectrometer, similar to that described by Fonck *et al.*,[18] employed 290-lines/mm (1700—120 Å) and 450-lines/mm (1100—100 Å) gratings, the dispersion elements being remotely interchangeable. The photoemissive surface of the microchannel plate detector was coated with CuI. The vuv instrument had not previously been calibrated against absolute photon flux. In the present experiments, however, the plasma emission itself was used to measure the relative spectral sensitivity function and the calibration placed on an absolute basis (at wave lengths >1200 Å) by reference to a standard luminosity source, namely, a MgF_2-window D_2 lamp, absolutely calibrated at the National Physical Laboratory of the United Kingdom. Charge-transfer recombination light from the nuclei of the light gases He, C, N, and O in ASDEX provided a convenient pattern of lines for spectral sensitivity measurements in the vuv region.

The visible spectrometers, with 1-m Czerny-Turner configurations, have a more limited wavelength coverage about a chosen central wavelength but have a correspondingly higher resolution than the vuv survey instrument. The spectrometer in the downstream position A had a 2160-line/mm grating while the spectrometer in the upstream position had a 1200-line/mm grating, both gratings being blazed for 5000 Å in first order. A variety of dispersions was therefore available from 0.18 Å/(OMA channel) in first order with the 1200-lines/mm grating to 0.05 Å/(OMA channel) in second order with the higher-resolution grating. The corresponding spectral coverages over 720 intensified channels were 130 and 35 Å.

III. CHARGE-EXCHANGE LINE INTENSITIES

The volume emissivity of the lines excited by charge exchange with neutral-beam atoms depends on the product of the neutral-beam density and the density $N(H^0)$ of the recombining impurity ion, viz.,

$$\epsilon_{CX}(\lambda)=N(H^0)N(Z)\langle\sigma_\lambda(nl,n'l')_{CX}v_b\rangle\ , \tag{1}$$

where $\sigma_\lambda(nl,n'l')_{CX}$ is the effective cross section for excitation of the nl-$n'l'$ transition in the recombining ion, $N(Z)$ is the density of the recombining ions with nuclear charge Z, and $eN(H^0)v_b$ is the beam current. Most typically in practice, the input beam current is known and its attenuation in the plasma can be calculated. Thus the ionic concentration $N(Z)$ can be derived if the effective CX cross sections are known, or alternatively, if $N(Z)$ can be deduced from other spectroscopic data, the CX cross sections can be derived. In this paper ionic concentrations are derived from the vuv CX data, and with the gross assumption that these concentrations are invariant over a number of similar discharges, an attempt is made to derive the poorly known effective cross sections for the visible CX lines. In order to proceed, however, the beam current at the viewing location of the spectrometers needs to be calculated. A first step in this analysis is to measure the beam energy components.

Following the technique used by Fielding and Stork,[19] D_2 gas at a pressure $\sim 10^{-5}$ torr was admitted to the torus chamber and the spectrally shifted H_α light arising from the resonance CX excitation of the fast energy components was monitored. The relative intensities of the H_α emission from the three beam components at E_0, $E_0/2$, and $E_0/3$ shown in Fig. 2 are proportional to the beam

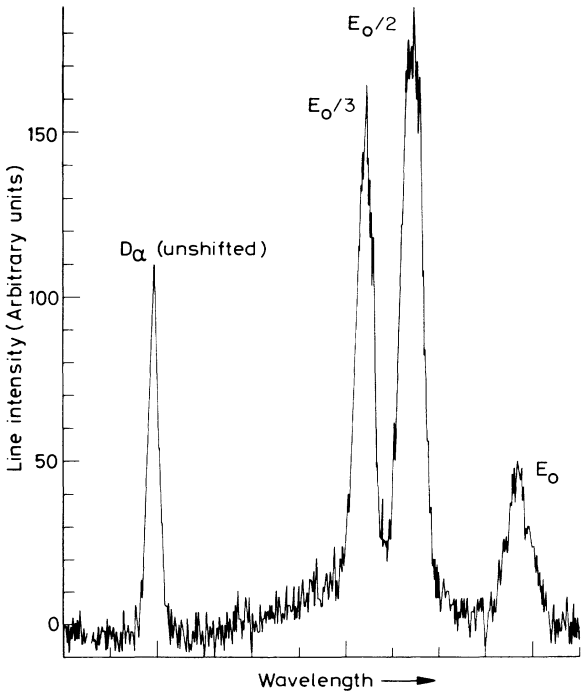

FIG. 2. The spectrum of D_α from a low-pressure (1.5×10^5 torr) D_2 gas filling in the torus irradiated by the SE beam of H^0 at $E_0=40$ keV. The Doppler-shifted charge-exchange lines from the three beam-energy components E_0, $E_0/2$, and $E_0/3$ have intensities proportional to the component beam fluxes. The power ratio E_0:$E_0/2$:$E_0/3$ is 0.41:0.44:0.15

fluxes $j(E_0/k)$ at these three energies ($E_0=41.5$ keV, $k=1,2,3$) after correction for the appropriate CX excitation rates.[19] The derived fluxes when multiplied by their beam energy give a relative power ratio for the beam components of 0.41 (E_0):0.44 ($E_0/2$):0.15 ($E_0/3$).

Model calculations of the beam attenuation, e.g., Isler *et al.*,[4] depend critically on the spatial profiles of the energy components of the fast beam and of the plasma density and less critically on the electron-temperature profiles. At the observation region in ASDEX, the fast-neutral-beam profile is well modeled by a single Gaussian on the major plane of the torus. The electron-density profile is of the form

$$n_e(r)=n_e(0)[1-(r/a)^{\alpha}]^{\beta},$$

where α and β are fit parameters ($\alpha\sim 3.5$, $\beta\sim 5$ typically) to the unfolded interferometric data. A radial-density profile during a discharge with neutral-beam injection is shown in Fig. 3. The attenuation of the input beam is primarily due to charge exchange and ionizing collisions with thermal protons when the beam energy is tens of keV and the electron temperature spans values from 100 eV $\leq T_e <$ 3 keV. Precise calculations taking into account charge-exchange collisions with impurity fractions and with the depleted proton density leave the attenuation due to CX practically unaltered since the CX cross sections scale almost linearly with Z. In the model calculations of the beam attenuation, electron and proton ionization of the beam neutrals are also taken into account and the total attenuation at the viewing position A is found not to exceed 25%.

The volume emissivity of a CX transition in an impurity ion, e.g., O VIII is given by

$$\epsilon(\lambda)=N(O^{8+})\sum_{k=1}^{3} j(E_0/k)\sigma_{\lambda}(E_0/k), \quad (2)$$

where $\sigma(E_0/k)$ is the effective cross section for CX excitation of a given wavelength λ. Using the attenuation code of Isler *et al.*[4] together with the CX cross sections of Shipsey *et al.*[7] and Green *et al.*,[20] the CX emissivity profiles of the three beam components of the $n=2$–3 transition in O VIII are shown in Fig. 4 together with their sum. A nominal 1% oxygen concentration relative to the electron density has been assumed in the model calculations pertinent to Fig. 4. In this paper we have made the working assumption that $N(Z)/n_e$ is constant across the plasma profile. Furthermore, in the intersection region defined by the viewing spectrometer, the electron temperature is sufficiently high [$T_e(0)\simeq 850$ eV in Ohmically heated plasmas and higher still in beam-heated plasmas] for the assumption to be valid that all the light impurities such as oxygen exist as bare nuclei and that all therefore will contribute to the intensity of the CX-excited lines of the H-like species. The emission profile is clearly a convolution of the impurity-density and beam profiles, and, as illustrated in Fig. 4, can be extremely asymmetric depending on the viewing position chosen.

A possible correction factor arises from the change in ionization balance due to charge-exchange recombination during the beam-injection period. This effect can be simulated by comparing the probability for CX recombination of the impurity nucleii, e.g., O^{8+} relative to reionization, $O^{7+}+e\rightarrow O^{8+}$, by electron impact during one transit of the ions around the torus. Since $\tau_{\text{transit}} < \tau_{\text{ioniz}} < \tau_{\text{CXR}} < \tau_{\text{beam pulse}}$, this probability ratio is just the steady-state ionization balance between CXR and electron-impact ionization. Assuming the nuclei are located on flux surfaces ($r\sim 15$ cm) and that there is no ra-

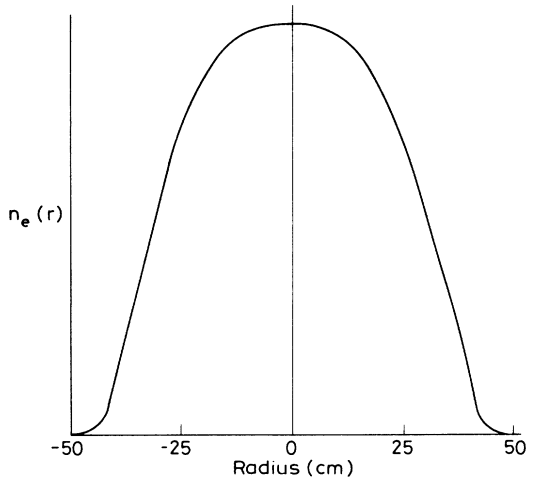

FIG. 3. Electron-density profile for an ASDEX discharge (No. 2) showing the relativity flat central region.

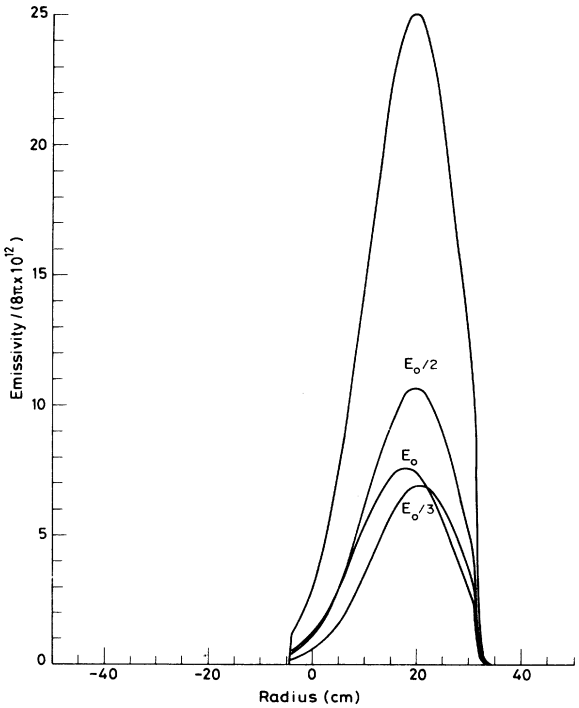

FIG. 4. The result of model calculations of the radial emissivity of O VIII ($n=3$–2) along the line of sight A (Fig. 1). The signal from the three energy components of the beam together with the total is shown for discharge No. 1.

dial diffusion within an ionization time ~ 0.7 ms, the relative probabilities scale as

$$\frac{P_{\mathrm{CX}}(\mathrm{recom})}{P_{\mathrm{el}}(\mathrm{ioniz})} = \frac{2L\left[\xi \sum_{k=1}^{3} N(\mathrm{H}^0, E_0/k)\sigma_{\mathrm{CX}}(E_0/k)v_i\right]}{4\pi Rq\langle\sigma_i(\mathrm{O}^{7+})v_e\rangle\bar{n}_e} = \frac{N(\mathrm{O}^{7+})}{N(\mathrm{O}^{8+})}, \quad (3)$$

where $L = 0.4$ m is the toroidal extent of the flux surface irradiated by each injected beam and $R = 1.65$ m is the major radius of the tokamak; σ_{CX} and σ_i are the charge-exchange O^{8+}-recombination and the electron-impact O^{7+}-ionization cross sections, respectively; and $\xi \sim 0.8$ is a factor taking into account the attenuation of the beam-injected neutral density $N(\mathrm{H}^0, E_0/k)$ as it propagates through the flux surface. The above ratio is of the order of 4% with both beams irradiating the plasma. The recombination due to the heating beams, *per se,* therefore does not materially affect the concentration of impurity nucleii though, of course, on a time scale considerably longer than an ionization time, other factors, such as cross-field transport and changes in the atomic influxes from the plasma boundary, may do so.

A second possible source of error relates to contributions from toroidally circulating ions which have been produced by charge-exchange recombination and which can in principle contribute to the "prompt" CX line intensity by electron-impact excitation. This "plume" effect[15] is most serious for the Lyman-series lines of low-Z ions, e.g., He^+. The magnitude of the plume contribution depends on the beam-injection and spectrometer-viewing geometry. In the present experiments the near-radial viewing position A, used for the quantitative derivation of impurity concentrations, minimizes the intersection with the circulating ions. For the nonresonance yrast transition in this study the effect of electron-impact excitation is small in comparison with the charge-transfer excitation at 40 keV/amu. The plume attenuation factor[15] being $\zeta = d/2\pi Rq = 2.5 \times 10^{-2}$ ensures that the plume effect is of minimal importance, where d is the intersection length of a magnetic flux tube through the beam-irradiated plasma viewed by the spectrometer, and $2\pi Rq$ is the circumferential length of the flux tube.

In the above model calculation, the cross section $\sigma_{\mathrm{CX}}(n,l)$ for occupying a given quantum state n,l has had to be converted into the effective cross section for the prompt emission of a photon $\sigma_\lambda(nl,n'l')_{\mathrm{CX}}$. This problem has been discussed by Fonck *et al.*[15] and by Isler.[5] In the simplest ("collision-free") case where there is no redistribution of the level occupancy following the recombination process, contributions to the effective cross section will arise from cascade electrons which decay spontaneously from upper levels whose initial populations will also be determined by charge exchange. In this calculation the A_{nm} values were encoded up to $n = 20$ from the tables for hydrogen published by Green *et al.*[21] More complex coupling between the levels is possible due to electronic collisions, and in the opposite (extreme) case of high collisionality the sublevels will be statistically populated. Sampson[22] gives the criterion for complete statistical mixing as

$$n_e \geq \frac{Z^{7.5}}{n^{8.5}} 1.18 \times 10^{15}\ \mathrm{cm}^{-3}. \quad (4)$$

For the plasma densities relevant to this study on ASDEX and for quantum levels $n \lesssim m$ in hydrogenic ions of the light gases, e.g., O and C, the complete statistical mixing model is inappropriate. This comment relates to CX excitation of the vuv emission lines. For sufficiently high quantum numbers, of course, statistical populations are to be expected and this condition could be relevant to some of the visible CX emission features. Summers[23] and Spence and Summers[24] have recently carried out more precise mixing calculations for the different $l+\frac{1}{2} \rightarrow l+\frac{3}{2}$, $l+\frac{1}{2} \rightarrow l+\frac{1}{2}$, $l-\frac{1}{2} \rightarrow l+\frac{1}{2}$ transitions in hydrogenic ions. In general these calculations confirm the general formula (4).

In a tokamak plasma environment motional Stark effects due to the thermal motion of the ions across the magnetic fields and Zeeman splitting will also alter the value of $\sigma_\lambda(nl,n'l')_{\mathrm{CX}}$ and n,l,j may no longer be good quantum state designations. These problems will affect equal-j states of the same principal quantum number in particular and will become increasingly important at high n. In the present analyses a "half-mixed" decay scheme is adopted[25] in which the almost degenerate states of equal j are mixed for $n < m$, while for $n > m$, all the levels are assumed to be statistically populated.

In addition to the first-order CX collisions with the fast-beam atoms, a second-order contribution to the CX signal is to be expected from those CX collisions which involve the thermal (~ 1 keV) neutrals produced by the first-order reactions. This "halo" contribution is not constrained to the beam-plasma interaction volume but will be spread throughout the plasma cross section. At thermal energies, high-n levels are not populated to any appreciable extent by charge-transfer collisions involving ground-state hydrogen atoms.[15] The halo correction will therefore only affect the vuv lines, and in particular the Balmer-α transition of the recombined nuclei. Assuming straight-line random trajectories for the thermal neutrals, the correction for the additional halo signal, in O VIII, $n = 3$–2, is calculated typically to be $\lesssim 20\%$ of that expected from the CX reactions involving the fast beam. In this study the absolute errors in the derivation of impurity concentrations, etc., exceed this fraction and the halo contribution has been neglected.

IV. RESULTS

A. The vacuum-ultraviolet spectrum

A sample 16-ms time frame of the vuv spectrum during the Ohmic-heating phase in ASDEX is shown in Fig. 5. The strongest features of the emission are mainly resonance lines from the light elements C, N, and O, from wall material such as Fe, and occasionally from S injected as H_2S for ion transport studies. The truncated spectral band, Fig. 6, shows schematically how the spectral

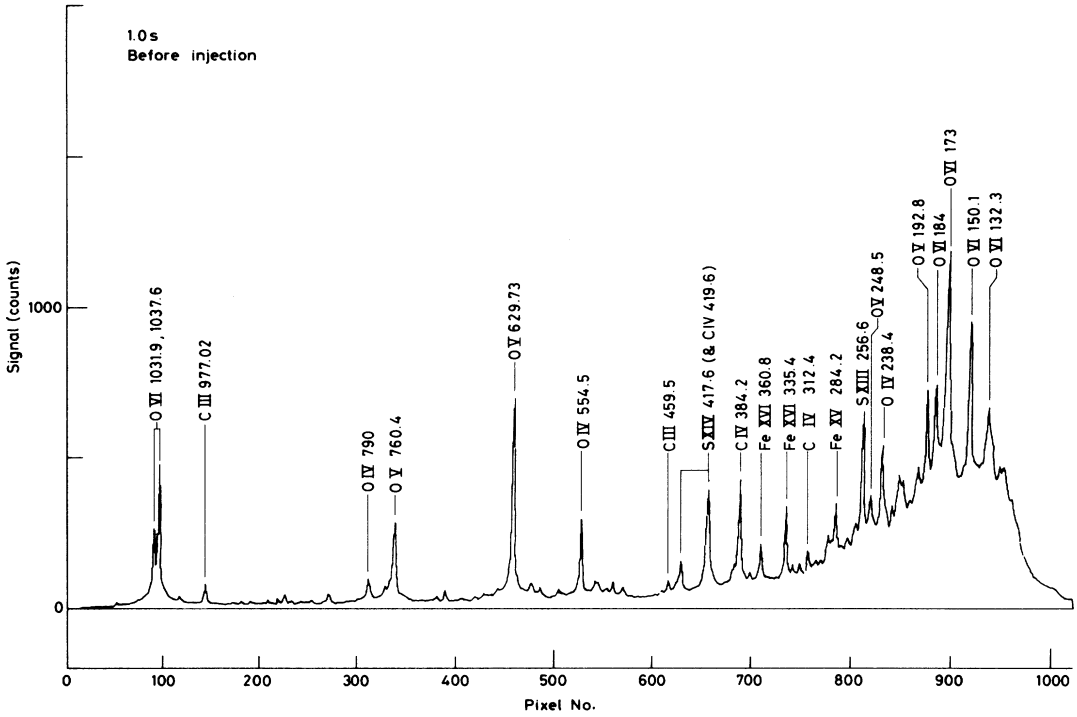

FIG. 5. Spectrum taken with the vuv survey spectrometer at 1s into the Ohmic-heating phase of ASDEX discharge. Exposure time is 16 ms. The pixel number refers to the reticon readout position. Approximately, with the 450-lines/mm grating, pixel $100 = 10^3$ Å and pixel $10^3 = 100$ Å.

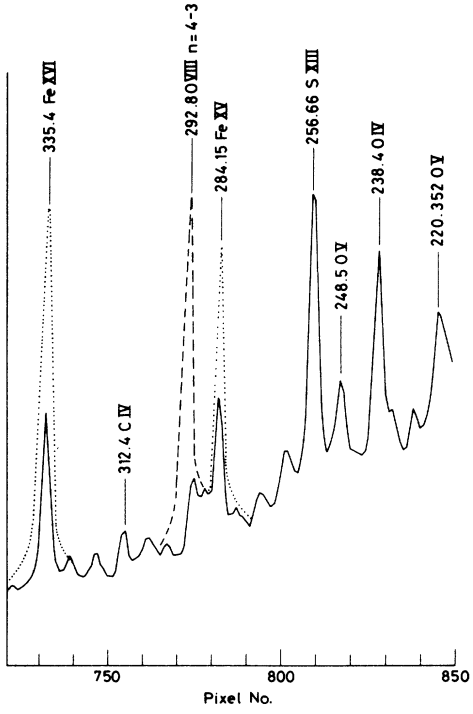

FIG. 6. Superimposition of spectral features with different heating modes in ASDEX. The dotted features are prominent during ICRH heating; the dashed features appear only during neutral-beam injection. The background (solid line) spectra are typical for Ohmically heated plasmas.

features change during different operating conditions in ASDEX. No ordinate scale is shown here since there is a considerable difference in the average signal level between Ohmic- and auxiliary-heated plasmas. The Ohmic spectrum, which may be regarded as the "basic" emission spectrum, is shown as a solid line in Fig. 6, overlaid by features which appear characteristically with the different heating methods. ICRH heating, for example, enhances the metal (Fe) spectrum. Charge-exchange-excited lines are only present during beam heating. Figure 7, for example, shows the full bandwidth covered by the 450-lines/mm grating at the end of the beam-injection pulse. The $\Delta n = 1,2$ transitions from O^{7+}, N^{6+}, and C^{5+} dominate the spectrum during the beam injection and rapidly disappear as the beam current is switched off (30 ms between time frames). Line blending is a problem with the limited resolution of the vuv instrument but in most cases the CX features are clearly registered. The O VIII $n = 4$—5 transition at 633 Å, for example, is quite distinguishable during beam injection from the neighboring strong line of O V at 629.73 Å, Fig. 7. The CX feature at 134 Å is unfortunately a blend of C VI, $n = 2$—4 at 135 Å and N VII, $n = 2$—3 at 134 Å. The minority C VI component of this line intensity can be assessed by reference to the strength of the C VI, $n = 2$—3 at 182 Å using the relative CX cross sections.[5] Identification of the weaker CX lines is made easier by dividing numerically the beam-on spectrum by the spectrum taken after the beam switch-off. We note that lines from hydrogenic ions of the light elements, in first, third, and fifth orders, can account for nearly all of the CX features identified in this

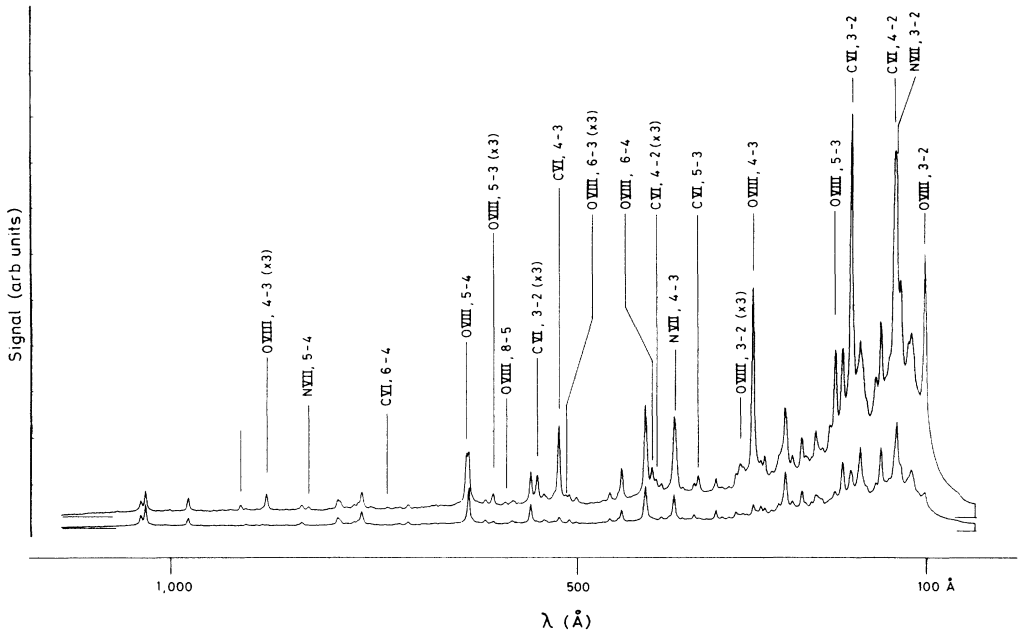

FIG. 7. The vuv survey spectrum (with 450-lines/mm grating) at two different times during an ASDEX discharge. The lower spectrum is taken at 1.4 s just after the switch off of the neutral beams. The upper spectrum is taken at 1.370 s during the beam injection. Exposure times for both spectra are 16 ms. All the features annotated are charge-exchange-recombination lines which appear only during the beam-injection period.

way.

In order to confirm that the CX line intensities mimic the beam current, the vuv instrument was also operated in the group-pixel (polychromator) mode. In contrast to the markedly different behavior of the resonance lines which, due to changes in ionization balance and transport, show intensity variations on a tens of milliseconds time scale throughout the discharge, the CX-excited lines (Fig. 8) decay abruptly in 1—1.5 ms following beam switchoff. A more detailed analysis of this sharp reduction in the CX intensities has been made by unfolding the detector phosphor decay time, using a maximum entropy approach.[26] The results, illustrated in Fig. 9, indicate a residual level with a much longer time constant which could be due to background continuum or line blending within the "monochromatic" pixel grouping chosen to represent the main CX line.

Following Isler and Langley,[5] the CX line intensities, when compared with their relative effective cross sections for their excitation, may be used to determine the spectral sensitivity curve for the vuv instrument. The inverse sensitivity is shown in Fig. 10 for the 290-lines/mm grating. The sensitivity curve is placed on an absolute basis at $\lambda > 1200$ Å by reference to a standard lamp. The 450-lines/mm grating, in turn, can then be determined by referring to the 290-lines/mm-grating CX data, assuming that the impurity concentrations do not change throughout a sequence of similar discharges. The spectral sensitivity has a maximum at 220 Å and its shape at this end of the spectrum can be derived with confidence from the CX results. At the long wavelength end, $\lambda > 700$ Å, the CX lines are weaker, the instrument less sensitive, and

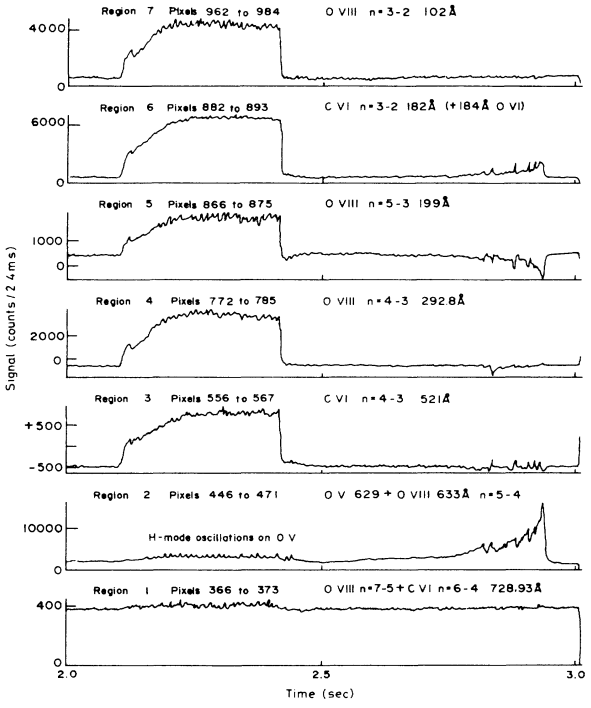

FIG. 8. The vuv survey spectrometer (with 450-lines/mm grating) operated in the polychromator mode showing that the intensities of the charge-exchange lines follow the neutral-beam-injection current. The background line emissions due to free-electron excitation do not show this sharp decrease in intensity following beam switchoff.

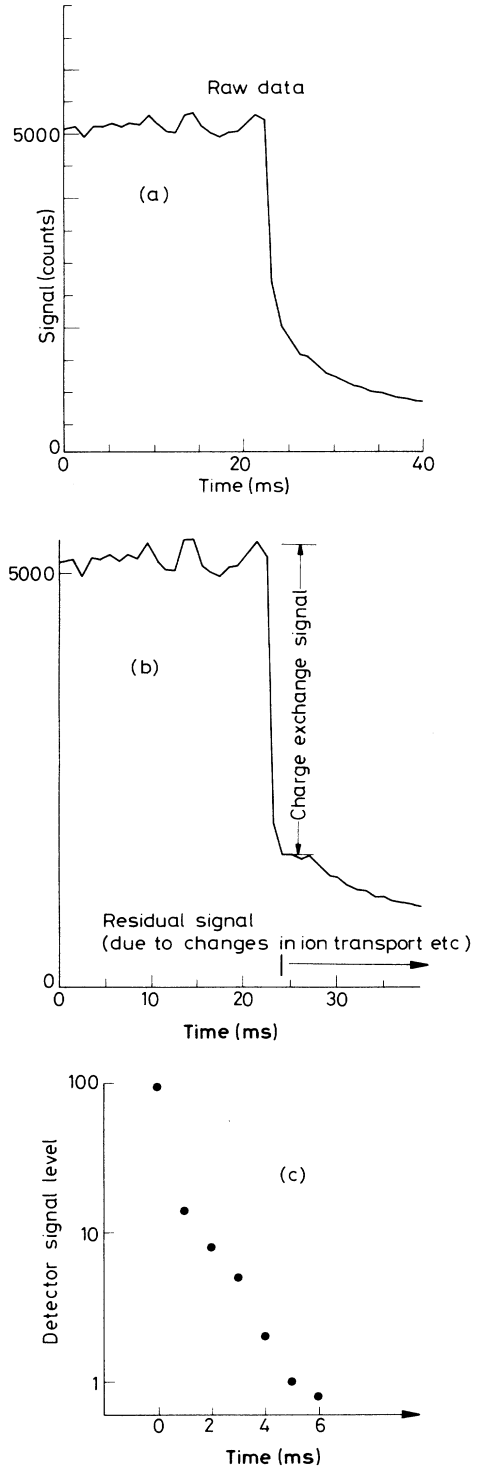

FIG. 9. (a) Time response of a typical CX line during neutral-beam switchoff measured by vuv survey instrument in polychromator mode. (b) After deconvolution of the phosphor decay, the charge-exchange signal shows a more abrupt step due to the cutoff of the neutral beam followed by a pedestal with a more gradual decay. This post-beam residual signal may be due to blended background line emission whose time variation is associated with ion transport and ionization balance changes. (c) Assumed inherent time response of detector.

the linkup with the absolute values from standard lamp results less convincing than had been hoped for.

Having calibrated the vuv spectrometer against absolute photon flux, it is then straightforward to measure the irradiance of those resonance lines which are prominent during the Ohmic-heating phase. Using an ion impurity transport code[27] to predict the line-of-sight depth for each of the emitting ion species, the volume emissivity and thence the impurity concentrations are derived in the same manner as described, for example, for the Joint European Tokamak (JET) plasma.[28]

Again, as for the JET plasma, the analysis is more secure for the more highly ionized metals than for the lighter elements, the former being in near-coronal ionization balance in the body of the plasma. The light elements emit in the vuv only from low ion stages located close to the plasma periphery and their derived central concentrations rely critically on the transport model.

Typical values for impurity concentrations derived from the resonance line intensities during Ohmic heating are as follows:

$$N(\mathrm{O})(\text{from O VI, } 2s\text{-}2p) = 4\times 10^{11}\ \mathrm{cm}^{-3} \sim 9\times 10^{-3}\, n_e(0)\ ,$$

$$N(\mathrm{S})(\text{from S XIV, } 2s\text{-}2p) = 5\times 10^{9}\ \mathrm{cm}^{-3} \sim 1\times 10^{-4}\, n_e(0)\ ,$$

$$N(\mathrm{Fe})(\text{from Fe XVI, } 3s\text{-}3p) = 1\times 10^{9}\ \mathrm{cm}^{-3} \sim 2\times 10^{-5}\, n_e(0)\ .$$

The oxygen concentration is high relative to that quoted recently[17] where the smaller values are perhaps more appropriate to a lengthy period of continuous tokamak operation and wall conditioning. One cannot, of course, assume that the impurity concentrations (above) apply during the beam-heating phase when impurity sources and ion transport are known to be modified. Accumulation of the impurities especially of the metals is a feature of improved confinement, which is observed in particular in the so-called "quiescent H modes," during beam injection.[6] However, the derived concentrations (Ohmic) provide a guide to those expected during "normal" beam injection when enhancement factors of between 4 and 10 are commonly experimenced.

In order to derive impurity (nuclei) concentrations in the hot core of the plasma during the beam-injection phase, we turn our attention to absolute intensities of the CX lines. The abrupt change in the CX signals following beam switch-off (Fig. 8) are proportional to the impurity ion densities at the end of the beam-heating pulse, and can be converted into absolute nucleii concentrations using the appropriate modeling code.[4] In fact, the survey spectral time frame near the end of the beam pulse, see, e.g., Fig. 7, represents a wider data set and this readout mode was more commonly used to derive absolute line intensities. These intensities, in units of irradiance (photons $\mathrm{cm}^{-2}\,\mathrm{s}^{-1}$) are shown in Table I for two separate discharges, Nos. 1 and 2, and are to be compared with the model calculations assuming a nominal impurity level of 1% of $n_e(r=0)$. Scaling the nominal concentration to fit

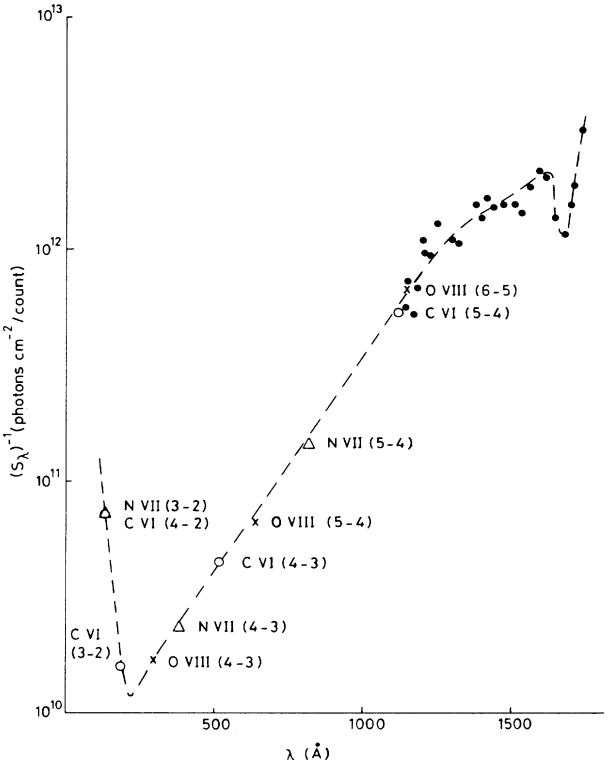

FIG. 10. Sensitivity of vuv survey instrument (290-lines/mm grating) based on the relative intensities of the CX lines at short wavelengths and normalized to the absolute sensitivity using a D_2 standard lamp at $\lambda > 1150$ Å. ○, C VI, △, N VII; ×, O VII; ●, D_2 lamp.

the observed irradiances yields the derived impurity concentration (Table I, right-hand column) relative to the central electron density $n_e(r=0)$. The concentrations are not completely self-consistent due to shot-to-shot variations in the data used to derive the instrument sensitivity and the line intensities shown in Table I. In addition, however, systematic errors may well have been introduced due to the subtraction of line blends and background light in the extraction of the monochromatic line intensity from the survey spectrum. The results indicate an oxygen enhancement over the Ohmic values which is not more than a factor of 2. Again, a factor of 2 encompasses the range of concentrations derived from separate beam-heated discharges. A value of the effective core ion charge $Z_{\text{eff}}=2.5$ is derived from the present analyses, whereas visible bremstrahlung measurements of Z_{eff} of the order 1.5 is more typical in ASDEX with beam heating.

B. The visible and quartz uv spectrum

Operating in the visible part of the spectrum offers many advantages in terms of instrument versatility, spectral resolution, and the availability of luminosity standards for absolute calibration. Furthermore, the use of optical components such as fiber optics, mirrors, and quartz windows enables spatial scans of the plasma emission and remote operation of the spectrometer from the torus vacuum system. However, the cross sections for CX recombination into the high $n > m$ states which are responsible for the visible CX transitions, are thought to be considerably lower than the values for $n < m$. Typically they are less by a factor like 10^{-2} at 40 keV/amu beam energy, and considerably less still at low beam energies of the order < 10keV/amu. As pointed out by Fonck *et al.*,[15] the absolute cross sections for CX recombination into high-n states are not well established either from model calculations or by experiment. With these points in mind and encouraged by the vuv results, a complete survey of the visible spectrum from ASDEX in the spectral region 2500–7000 Å was undertaken.

Standard, beam-heated discharges in D_2 and in He were studied while the beam particle energy per amu could be changed by switching from H to D injection. Several strong CX line features are observed which can be attributed to recombination with O, N, C, and He nuclei. Spectral surveys in the vicinity of the principal He II, C VI, and O VIII Lines are shown in Figs. 11, 12, and 13. The He II spectrum was recorded with He as the working gas while the C VI and O VIII spectra were intrinsic impurities in a D_2 plasma. The He II spectrum was obtained while commissioning the visible spectrometer on viewing line *A*. A later improvement in the sensitivity of the apparatus

TABLE I. CX radiances in the vuv from ASDEX and deduced impurity concentrations. 1 gigarayleigh = 1 GR = 10^{15} photons cm^{-2} s^{-1}.

Element	Transition	Wavelength (Å)	Experimental irradiance (GR) No. 1 450/mn grating	Experimental irradiance (GR) No. 2 290-g/mm grating	Model irradiance from CX code (1% concentrations of impurity assumed) (GR)	Impurity concentrations relative to central electron density No. 1	Impurity concentrations relative to central electron density No. 2
O	$n=2$-1	19			18.2		
O	$n=3$-2	102	32.4		12.1	1.06%	
O	$n=4$-3	293	29.3	22.1	10.7	0.98%	2.13%
O	$n=5$-4	633	28.7	21.1	11.8	0.80%	1.86%
O	$n=5$-3	200	8.0		4.8	0.78%	
C	$n=3$-2	182	59.9	24.8	7.41	3.28%	4.08%
C	$n=4$-3	521	39.7	24.4	8.87	1.92%	2.73%

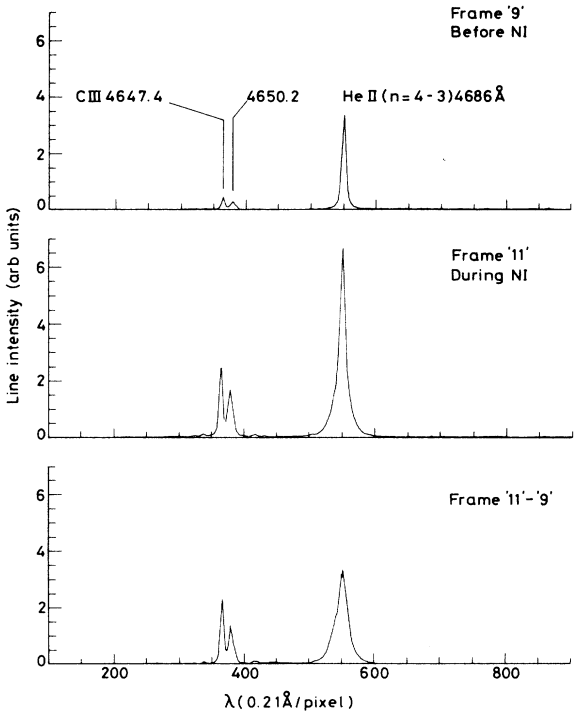

FIG. 11. Time sequence of He II ($n=4$—3) emission prior to and during neutral-beam injection (viewing geometry A). Subtraction of the first two frames yields (below) the broadened CX contribution to the line intensity.

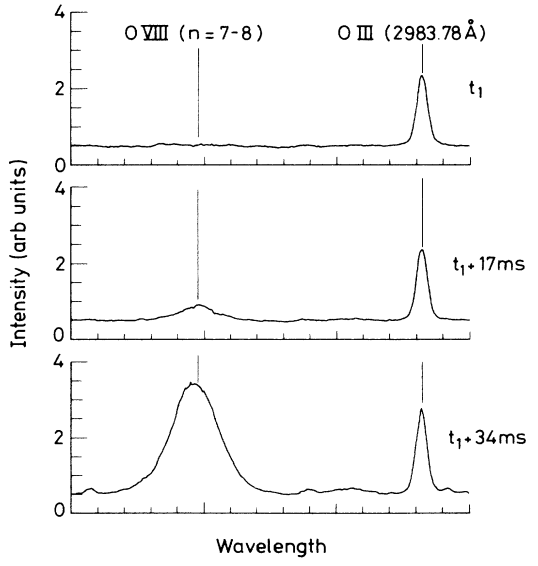

FIG. 12. Time sequence of O VIII ($n=8$—7) emission prior to (t_1) and during beam injection (t_1+17 ms and t_1+34 ms). The breadth of the CX feature, relative to that from the recycling edge lines, e.g., O III, as well as its temporal variation are important features of the CX signature. (Viewing geometry A.)

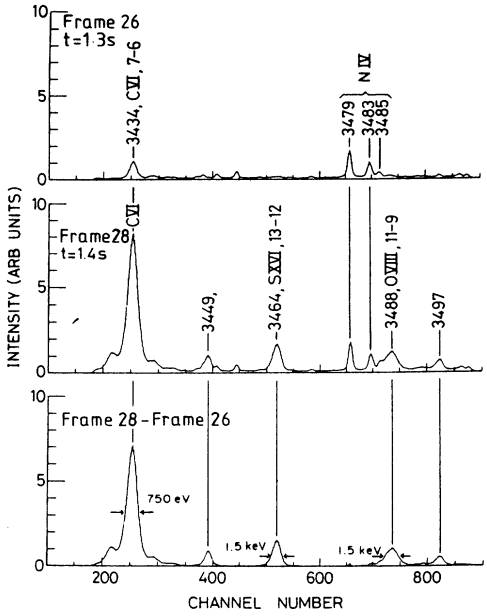

FIG. 13. Time sequence of CX emission in a portion of the visible spectrum. The top frame indicates the emission prior to beam injection, the middle frame illustrates the complexity of the CX features appearing during beam injection, and the bottom frame, derived from subtraction of the above two frames, gives the resultant CX features. (Viewing geometry A.)

was effected by optimizing the mirror viewing optics and changing the grating from a 1200-lines/mm holographic grating to a 2100-lines/mm ruled grating blazed for 5000 Å. Thus we now would expect for a D_2 plasma seeded with only 1% He to have the same CX signal-to-noise ratio as shown in Fig. 11.

As with the vuv lines the spatial and time dependence (see later) of the Rydberg transitions in the visible region are uniquely identified with their charge-exchange character. In the visible region, however, an additional identifying feature of the CX lines is their large spectral widths relative to neighboring lines. The latter are emitted from the cool plasma boundary where the temperature is typically $\lesssim 50$ eV whereas the CX lines exhibit mass motion and thermal broadening characteristic of the bulk of the plasma. Figure 12, for example, illustrates the spectral width and temporal difference between O VIII $n=7$—8 and a neighboring O III line at 2983.78 Å during the beam switch-on phase.

Figure 13 illustrates several interesting features within a relatively narrow spectral region. In addition to the C VI $n=7$—6 line at 3434 Å we can also observe a $\Delta n=2$ line from O VIII $n=11$—9 at 3488 Å and a line, tentatively identified as S XVI $n=13$—12, at 3464 Å. Ion temperatures of ~ 1.5 keV, obtained from the Doppler widths of the O VIII ion emission and from the S XVI line agree within experimental error, while that from the C VI line is smaller at ~ 750 eV. A single Gaussian fit to the C VI line, shown in Fig. 14, indicates that the line is a composite of the CX C VI $n=7$—6 line blended with other, possi-

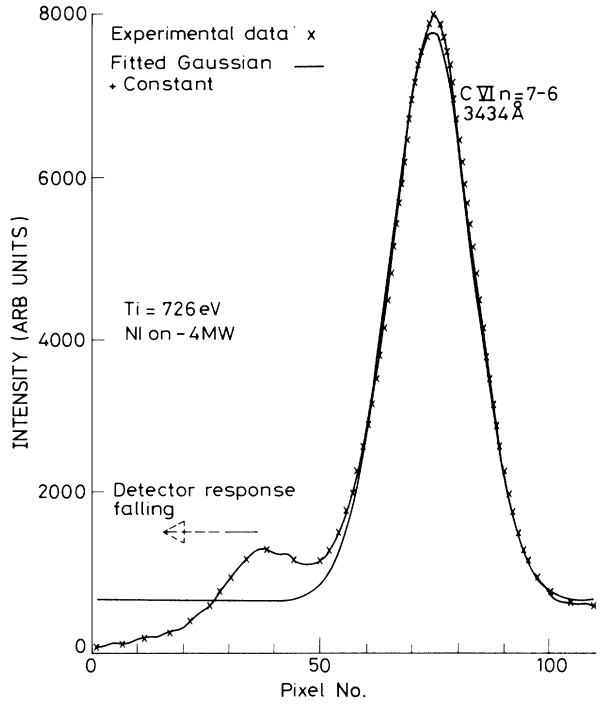

FIG. 14. Gaussian fit to the C VI ($n=7-6$) CX feature (viewing geometry *A*.)

bly CX, emission from outside the beam-interaction region. Positive identification of the lines at 3449 and 3497 Å have not been made but, in common with several similar weak features seen in the visible region only during beam injection, they appear to have a genuine CX signature. The time dependence of their intensities differs markedly from, say, the N IV triplet, Fig. 13, which is present before the neutral injection pulse. The weak line at 3430 Å is probably F IX $n=9-8$. Supporting evidence for this identification is given by spectra, Fig. 15, taken when the plasma vessel was contaminated by fluorine from insulating material (Teflon) during titanium-gettering experiments. In Fig. 15 the F IX intensity is comparable with that from C VI.

It is clear also that the CX spectra are not confined to hydrogenic species of the light elements. Heavier elements like Ti, Fe, Mo, and other metals do occur with relatively high abundancies in the He- or Ne-like stages in the plasma core at typical tokamak temperatures. Identification of these elements by means of CX recombination leads to a search for the corresponding lines from the Li- and Na-like ions. We report here on the first CX-recombination spectra from Li-like sulfur and Na-like krypton. A more detailed analysis of these experiments will be published elsewhere.[29] The investigations were made by puffing H_2S or Kr into the discharge during the NBI heating phase. The gases were added at a constant rate over periods of between 200 and 300 ms. Concentrations of S and Kr thus achieved are estimated at 10^{-3}–10^{-2} of the electron density. In the case of sulfur all $\Delta n=1$ transitions of the Li-like ions in the range $2500<\lambda<7000$ Å, i.e., $n=11-10$ to $n=15-14$, have been observed. In the same way all seven transitions $n=16-15$ to $n=22-21$ of Na-like Kr could be found. As an example (Fig. 16) the appearance of the $n=11-10$ line of S^{+13} after switching on the NI beam at $t=1.10$ s is due to the residual amount of sulfur which remained from puffing into previous discharges. Following an injection of H_2S at $t=1.25$ s, the intensity is seen to increase and Doppler profiles with linewidths of ~ 2 Å (yielding $T_i \sim 3$ keV) have been recorded.

Electron temperatures in these discharges were measured to be relatively low, $T_e(0) \sim 1.5$ keV. At the intersection position of the NI beam and the line-of-sight of

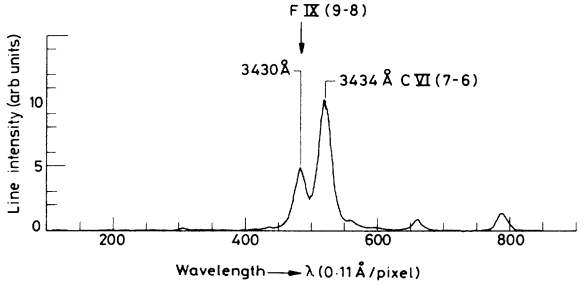

FIG. 15. Illustration of the additional F IX CX line on the blue wing of C VI ($n=7-6$) during beam injection when fluorine is a contaminant in ASDEX (viewing geometry *A*.)

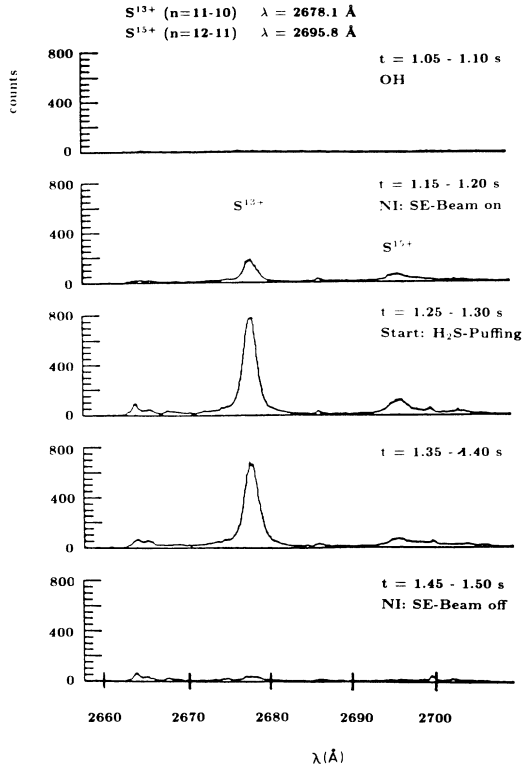

FIG. 16. Charge-exchange features of sulfur in the visible region when H_2S is added as trace gas to ASDEX (viewing geometry *A*.)

the upstream spectrometer B ($r \sim 25$ cm, see Fig. 1), T_e is approximately 0.6 keV. At these low temperatures the majority of sulfur ions are expected to be in the He-like state ($\gtrsim 90\%$), whereas the completely ionized atoms are in the minority (a few percent only). For this reason the H-like CX lines, such as the $n=12-11$ line of S^{15+} in Fig. 16, are weak.

Comparing H-like with Li-like atoms, we have to note that in the latter three-electron systems the energy degeneracy with respect to the orbital quantum number l is at least partly removed. In the case of high l ($l \sim n-1$) the outer electron is in nearly circular orbits and the energy levels are thus very close to those of H-like atoms with effective charge number $Z-2$. Conversely, in the case of low l we have highly eccentric orbits with less-screened nuclear charge. For the Li-like S^{+13} transition $n=11-10$ shown in Fig. 16 the $l \rightarrow l-1$ components are predicted to be shifted by as much as 125 Å for the lowest l with respect to the high-l (≥ 7) components. The latter, for ($Z_{\text{eff}}=Z-2=14$), coincide within $\Delta\lambda=0.3$ Å with the H-like wavelength $\lambda=2678$ Å. For intermediate values of l, e.g., the 3-2 satellite lines, still-large shifts of $\Delta\lambda=-5.5$ Å are predicted in the experiments; however, no strongly shifted components nor closer satellite lines could be observed, this being the case for the Li-like S^{13+} lines as well as for the Na-like Kr^{25+} lines. In the case of the Na-like spectra, qualitatively the same effects are to be expected. The centroids of the detected lines agree well with the H-like approximations for $Z_{\text{eff}}=Z-2$ and $Z_{\text{eff}}=Z-10$, respectively.

The O VIII spectra are particularly interesting, not only in the context of plasma diagnostics, but also because of our observations of high ($n=11$) quantum state populations. Hitherto, the line at 2976 Å $n=8-7$ has been used by other authors[10] as a diagnostic indicator of ion temperature and plasma rotational velocity. Scant regard has been given in the literature to the 4340-Å $n=9-8$ line of O VIII because of its proximity to H_γ and D_γ, while the 6068-Å $n=10-9$ line, as far as we know, has been completely ignored. The 2976-Å line, Fig. 12, is well separated from other lines and is an excellent candidate for plasma diagnostics but does suffer unacceptable attenuation when ducted through long, ~ 100-m, fiber-optic links as in the JET experiment.[30] Blending of H_γ and D_γ with the O VIII 4340-Å line is more of a nuisance than a serious limitation since the CX feature can often be unfolded by spectral subtraction techniques and multiple Gaussian fits. This task is further eased by viewing the beam-interaction region at an appropriate angle so as to shift spectrally the CX feature from the hydrogen edge emission wavelengths in response to the bulk plasma rotation. Perhaps the most significant observation[31] with the widest diagnostic potential is the O VIII $n=10-9$ line at 6068 Å, Fig. 17. In this illustration of a single time frame during beam injection viewed along line-of-sight B, the 6068-Å line is compared with the narrow fiducial lines from a neon lamp which are used as fixed wavelengths markers during the NI heating pulse.

The weak CX feature on the far red wing of the 6068-Å line is tentatively identified as N VII $n=12-10$. In comparison, the neon linewidths indicate the resolution of the

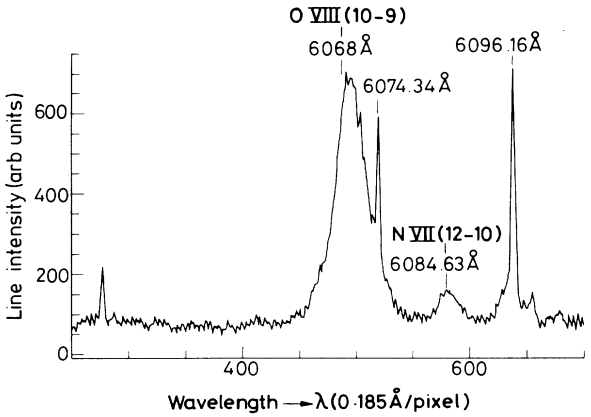

FIG. 17. Charge-exchange line of O VIII (10—9) superimposed on neon lamp lines. The narrow neon lines indicate the instrument function and act as wavelength markers from which the mass motion shifts can be derived (viewing position B.)

spectrometer. Toroidal rotations as high as 3×10^5 ms^{-1} have been recorded from the spectral shifts of the O VIII lines, during injection at a beam power of 4 MW. With viewing line B, the analysis of the line profiles, Fig. 17, is complicated by plasma effects such as rotational shear in the viewed plasma volume as well as thermal broadening. Moreover, at visible wavelengths, Zeeman splitting and polarization should be included in the line-shape analysis. Stark splitting due to the electric fields ($\sim 3\times 10^5$ V/m) seen by the ions as they gyrate about the magnetic field is of the same order or larger than Zeeman splitting and together these effects will exceed the separation of the more intense $nl \rightarrow n'l'$ transitions as shown, for example, for the $n=10-9$ line in Fig. 18. However, the total range of wavelengths spanned by the fine-structure components greatly exceeds the wavelength splitting due to Zeeman and Stark effects so that the overall shape of the observed spectral feature is more influenced by the population distribution of the l states and their decay rates. As confirmation, the shape of the 6068-Å CX line remained unaltered after transmission through a polarizer. Ion-ion col-

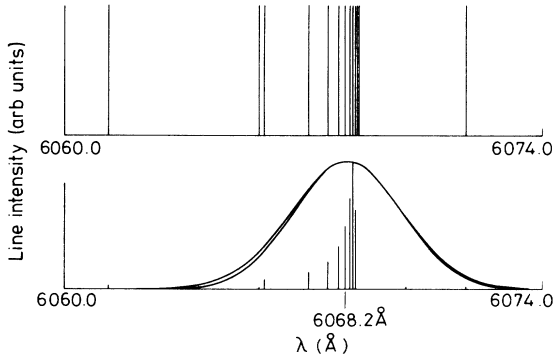

FIG. 18. Fine-structure components of O VIII (10—9), the inclusion of which distorts the thermally broadened profile at $T_i=1$ keV.

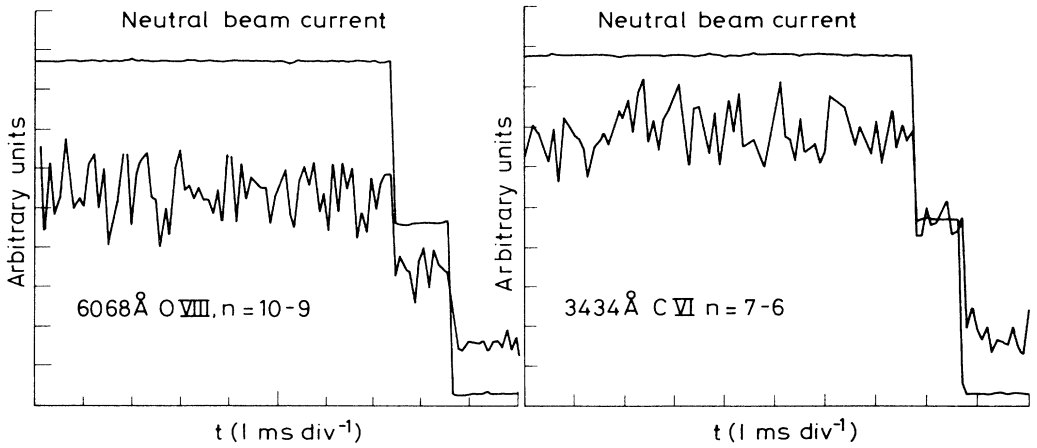

FIG. 19. Time response of charge-exchange visible lines with respect to the neutral-beam current.

TABLE II. Charge-exchange-recombination lines in the range $\lambda = 2500-8000$ Å observed from ASDEX.

Element	Transition	λ (Å)	Relative intensities from spectral response (a.u.)	Comments
He II	$n=4-3$	4686		
	$n=5-3$	3203.25		a
	$n=6-4$	6560.10		Could be blended with a, D_α
	$n=7-4$	5411.52		a
C VI	$n=7-6$	3434	38.4	a
	$n=8-7$	5291	28.5	a
	$n=9-8$	7717	13.3	a
N VII	$n=8-7$	3887	5.0	
	$n=9-8$	5669	10.0	a
	$n=10-9$	7926	4.2	a
	$n=12-10$	6085	2.0	
O VIII	$n=8-7$	2976	70.0	a, Good line for profile and intensity analysis
	$n=9-8$	4341	14.1	Blended with H_γ
	$n=10-9$	6068	17.7	a, Good line for profile and intensity analysis
	$n=11-9$	3488	5.5	
F IX	$n=9-8$	3430		
S XVI	$n=13-12$	3464	16.6	
	$n=12-11$	2695.8		
S XIV	$n=11-10$	2678		
	$n=12-11$	3521		
	$n=13-12$	4524.5		
	$n=14-13$	5702		
	$n=15-14$	7068		
Cl XVII	$n=13-12$	3067	25.0	
Kr XXVI	$n=16-15$	2504		
	$n=17-16$	3021		
	$n=18-17$	3605		
	$n=19-18$	4206		
	$n=20-19$	4990		
	$n=21-20$	5798		
	$n=22-21$	6689		

[a]Profile analysis requires deconvolution from residual pre-NI signal and/or from line blending.

TABLE III. Visible CX irradiances from ASDEX and deduced impurity densities. 1 GR $=10^{15}$ photons $cm^{-2} s^{-1}$ and n_c is the principal quantum number above which statistical mixing of the l states is assumed in the model calculations.

Transition	Experimental irradiance (GR)	Prediction of CX code with the assumption of 1% ionic concentration relative to n_e (GR)	Derived concentration (relative to n_e) (%)
C VI $n=7-6$ (wavelength is 3434 Å)	0.185		
$\sigma_\lambda(7-6)_{CX}$, Ref. 33, $n_c=7$		0.131	1.41
$\sigma_\lambda(7-6)_{CX}$, Ref. 34, $n_c=7$		0.068	2.72
$\sigma_\lambda(7-6)_{CX}$, Ref. 33, $n_c=8$		0.308	0.60
$\sigma_\lambda(7-6)_{CX}$, Ref. 34, $n_c=8$		0.076	2.43
O VIII $n=8-7$ (wavelength is 2977 Å)	1.46		
$\sigma_\lambda(7-6)_{CX}$, Ref. 33, $n_c=9$		0.495	2.95
$\sigma_\lambda(7-6)_{CX}$, Ref. 34, $n_c=9$		0.150	9.73
$\sigma_\lambda(7-6)_{CX}$, Ref. 32, $n_c=9$		0.511	2.86

lisions for these high quantum states such as $n=10,9$ in O VIII ensure that the l states are almost completely statistically populated.[24] An important consequence of the electric and magnetic fields arising from the plasma environment is that the levels will be driven into statistical populations even more readily than in a field-free situation. Precisely because the high quantum levels are in or near statistical equilibrium, then *any* populating process, be it CX recombination into $l \simeq m$ levels or electron-impact excitation, e.g., from the ground-state $1s\,^2S_{1/2}$ to the $n=10$, $l=1,2$ states, will result in the appearance of yrast transitions. It is therefore of even more significance in the case of the visible lines to confirm their CX character by their temporal correlation with the neutral-beam current.

A photomultiplier detector was used on the viewing line B spectrometer to monitor the detailed time evolution and decay of the $\Delta n=1$ transitions in C VI and O VIII. The frequency response of the detector (up to 10 kHz) was sufficient to follow the rapid switch-off of the beam current and to differentiate therefore between CX excitation and electron-impact effects following ionization balance changes which take place on a much longer time scale, typically 10^{-3} s or longer. The upper bound of the detector response resulted from the insertion of a 10-kHz filter which improved the signal-to-noise ratio of the photomultiplier without severly compromising the time response. Both the photomultiplier signal and the sum of the voltages from the four sources of the viewed neutral beam were fed into a LeCroy 8210 analog-to-digital converter. A 100-μs sampling time was used to produce the time histories as shown, for example, in Fig. 19. In this figure the neutral-particle beam is terminated by switching off successively each of the two pairs of sources. The double step in the line intensities is closely correlated with the beam current on a 0.1-ms time scale, thus uniquely identifying the lines as CX features.

Having established from their wavelengths, from their spectral broadening, and from their correlation with the beam current that the visible lines annotated in Table II are definite CX features, we can now proceed to relate their absolute irradiances along viewing-line A to effective cross sections for CX excitation into high quantum states. The experimental results, averaged over several discharges, are shown in Table III. The data have been analyzed for several cascade-corrected models ranging from an unmixed decay through the "limited $\Delta j=0$ mixed" model to the "half-mixed" model. In Table III we note the critical quantum state n_c above which statistical mixing is assumed. For the oxygen $n=8-7$ transition the data of Fritsch[32] and Ryufuku[33] give a very reasonable impurity concentration relative to an electron density without introducing statistical redistribution in the l levels. The cross section from Olson[34] gives an emissivity which is five times too low. For carbon, the cross sections from Olson[34] give reasonable results, as do the results of Ryufuku[33] using the onset of statistical mixing at $n_c=7$. Without an independent measurement of the impurity density, it is difficult to decide which model is correct. Assuming invariant impurity concentrations from the vuv sequence of discharges to the later visible sequence, the agreement for oxygen and carbon between the vuv data, Table I, and the visible data, Table III, is reasonable considering the factor-of-2 variations which appear within the vuv data set.

We now turn our attention to the spectral broadening of the CX feature as seen along viewing-lines A and B. The downstream viewing-line, A in Fig. 1, is practically along the torus major radius and so will not register toroidal rotation. The shape of the lines is adequately interpreted in terms of thermal broadening with ion temperatures typically in the 1–2 keV range. Viewing-line B, on the other hand, accommodated a large component of any toroidal motion and in consequence the spectral lines suffered time-varying shifts during the injection pulse which were of the same order as the thermal broadening. Unfortunately, rotational shear in the viewed plasma interaction region makes it difficult to describe a unique value to the toroidal momentum in the plasma. The toroidal rotation in ASDEX reaches a value of $\sim 3\times 10^7$ cm s^{-1}, the exact

value depending on the disruptive magnetohydrodynamic behavior in the plasma. The results, however, are consistent with the vuv CX spectral widths measured on DITE.[14]

V. DISCUSSION

Neutral-beam injection into the ASDEX tokamak has been shown to produce a rich spectrum of charge-exchange lines extending from the vuv into the visible. The most intense lines are, as expected, the $\Delta n = 1$ yrast transitions resulting from charge-exchange recombination of impurity nucleii such as O^{8+}, N^{7+}, and C^{6+}. In the vuv survey spectra, taken in relatively low resolution, line blending is a problem but nevertheless all of the expected CX features from these elements have been identified. In the visible region many CX lines have been identified in H-like C, N, O, F, S, and Cl, and several have been noted to have diagnostic potential.

There remain in the visible spectrum, however, many other weaker line features which also exhibit all the characteristics of charge-transfer recombination but which still remain unidentified. It is clear that the long-wavelength lines have considerable potential for exploitation as diagnostic indicators of mass motion and thermal broadening, these parameters being conveniently isolated with different but simultaneous viewing chords. An extension of this work using the C VI $n=8$–7, O VIII $n=10$–9, H_α, and He II $n=4$–3 transitions in JET during H_0 beam injection into JET has recently been carried out.[35]

The analysis of the visible CX line intensities in terms of impurity fractions also appears promising. The actual values for the effective cross sections of high quantum states $n > m$ are not well established and they vary sensitively with the relative velocity of the colliding particles. In the high-energy range with impacting velocities greater than 2.2×10^8 cm s^{-1}, a n^{-3} "rolloff" in the cross section

$$\sigma_{CX}(n,l)=\sigma_{CX}(m)\left|\frac{m}{\bar{n}}\right|^3, \tag{5}$$

i.e., the Oppenheimer rule,[36] appears to be moderately accurate. The n^{-3} dependence, however, does not provide a smooth correspondence with the calculated data such as those provided, e.g., by Olson[34] for the high quantum states. This problem is presently being pursued by the authors using the charge-exchange-recombination spectrum of He^{2+} in the ASDEX tokamak where a $n^{-\alpha}$ rolloff, $\alpha\sim2.5$, is indicated. From the present work at 40-keV injection energy, it appears that the close-coupled atomic-orbital model[32,8] gives the most consistent interpretation at $n > m$.

A complication which has been noted in this study and by others[10] relates to the C VI lines, e.g., $n=7$–6, Fig. 14. Such lines can have appreciable intensity outside of the irradiated plasma volume and are present even without beam injection. In the 20-keV beam-injection DITE tokamak[9] the "residual" C VI intensity, i.e., that which remains after accounting for charge exchange with the atomic beam on C^{6+}, is adequately explained by electron-impact excitation of C^{5+}, the spatial ionic population of which is modified by charge-transfer recombination with the background thermal neutrals. In the present experiments with higher beam energy the residual signal is less than in the DITE experiment, though CX with background thermal neutrals before and after the atomic injection pulse might still play a role. The situation with the C VI lines is complicated by possible blending with the same principal quantum jump in Li-like O VI. The latter can result from charge transfer between H^0 and O^{6+}. In the case of Rydberg states, blending of lines from several different ion species is always a potential problem but this is especially so for charge exchange with ions whose charge states are equal such as ion Z with a charge state of $(+z)$ and ion $Z+2$ with a charge state of $(+z)$ and is particularly relevant to C^{6+} when O^{6+} is a major impurity species. The fine-structure splitting in the Li-like ion results in several widely separated O VI line components, the identification of which, in principle, can establish the presence of this ion. In the $n=7$–6 transition of O VI, for example, the $7p$–$6s$, the $7d$–$6p$, and the $7i$–$6h$ transitions lie at 3067.4, 3313.9, and 3433.9 Å, respectively. However, with collisional mixing of the l states, the weighting of the yrast decay is heavily biased towards $\Delta l=1$, $l\sim n-1$, leaving the 3434 Å as by far the most intense component. The viewing geometry on ASDEX ensures that the 3434-Å emission is mainly due to charge exchange with the core concentration of C^{6+} rather than with the near-edge plasma concentration of O^{6+}. A "line-of-sight" tangential to the plasma periphery would have emphasized the O^{6+}.

In order to demonstrate that coincidences in wavelength due to transitions between Rydberg levels in different elements is a problem in tokamaks, a separate experiment was performed on the DITE tokamak. Adopting a similar visible spectrometer to that used on ASDEX, it was first established that the O VIII ($n=10$–9) line had no measurable intensity during Ohmic-heating discharges. Following injection of a gas puff of neon, however, a prominent line identified as Ne VIII ($n=10$–9) at 6068.2 ± 0.2 Å was observed with a spectral width corresponding to an ion temperature of 300 eV along with narrower neon lines from the plasma edge. The wavelengths O VIII ($n=10$–9) and the observed Ne VIII ($n=10$–9) transitions are coincident within the thermal width of the neon ion; the mechanism by which the $n=10$ level of Ne VIII is populated in ohmically heated plasma has not been established. Charge-exchange recombination into excited background hydrogen $H^{0*}+Ne^{8+}\rightarrow H^+ + (Ne^{7+})^*$ is a strong possibility since He-like impurities are pervasive ion species in tokamaks and have appreciable concentrations even in the outer regions of the plasma. Whatever the populating mechanism, however, it is clear that Rydberg-level coincidences between ion species such as H-like ion Z with a charge state of $(z-1)+$ and ion $Z+2$ with a charge state of $(z-1)+$ are likely to cause confusion in the absence of beam injection.

A further consideration is the effect on the effective charge-exchange cross section of excited states, e.g., H^{0*} ($2l$, etc.) in the impacting atom. This has been highlighted recently by Rice *et al.*[37] who ascribe the "anomalous" intensity of the high numbers of the $1s^2$-$1snp$ series in

Ar^{16+} to charge-transfer recombination between Ar^{17+} and the finite excited-state populations of background thermal atomic hydrogen in the region of the plasma edge. In the present experiments excited states of the thermal halo neutrals and of the background atomic hydrogen can contribute, in principle, to the total CX cross section into the upper levels, favoring those levels with $n = m' \cdot n^*$, where n^* is the excited state of the atomic hydrogen. For charge transfer between $H^{0*}(n=2)$ and O^{8+}, the preferred level for CX would be $n \sim 10$. An assessment of the excited-state contribution can be made from the relative magnitudes of the populating processes for $n > m'$; viz.,

$$R \simeq \frac{N(H^0)_b \alpha_{CX}(E_b) N(O^{8+})_b L_b + N(H^0)_b^* \alpha_{CX}(E_b^*) N(O^{8+})_b L_b}{N(H^0)_h^* \alpha_{CX}(E_h^*) l_h N(O^{8+})_h + N(H^0)_r^* \alpha_{CX}(E_r^*) l_r N(O^{8+})_r} , \tag{6}$$

where R is the ratio of the beam signal to the total charge-exchange signal from excited states of halos and background neutrals present due to recycling at the plasma edge. The subscripts b, h, and r refer to the particle densities and CXR rates, α_{CX}, in the beam interaction region, in the halo volume, and in the volume of the recycled atoms, respectively. The starred quantities represent excited-state populations in atomic hydrogen. The L,l symbols are the plasma depth viewed through the beam and the thermal atoms, respectively. Two sources of thermal hydrogen need to be considered, namely, the background thermals which recycle at the plasma boundary and whose concentration in the plasma core in ASDEX is several orders of magnitude less, typically, than that of the beam neutrals. The second source of the thermal neutrals is the beam halo whose concentration can be within an order of magnitude of the beam atoms. The cross sections for charge-transfer recombination into Rydberg states of impurity nucleii from excited (n^*) states of atomic hydrogen relative to that from the H^0 ground state scales approximately as $n^{*4}/|m/mn^*|^3$, i.e., $\sim n^{*7}$. Excited atomic states are therefore highly efficient at transferring electrons to levels (for example, $n=10$ in O VIII) which give rise to visible CX emission. In steady-state conditions with $n_e \sim 5 \times 10^{13}$ cm^{-3} and $T_e > 10$ eV, the $n=2$ level in hydrogen has a population which exceeds 1% of the ground-state population, about a quarter of this being in the $2\,^2S_{1/2}$ metastable state. These simple arguments therefore indicate that there is good reason to be concerned with the contribution to the CX visible signals from excited hydrogen. However, regarding the halos, a consideration of the relative mean free paths for excitation versus charge transfer indicate that these $\sim$1-keV-energy neutrals suffer one or more CX collisions typically before being lost from the plasma. Their lifetime within the body of the plasma is too short, by at least an order of magnitude, for excited-state populations to become established. Thus the factor $N(H^0)_h^*$ in the above equation for R is negligibly small and the effect of halo excited states can be dismissed in the ASDEX experiment. The slow-recycling hydrogen atoms at the plasma boundary, on the other hand, can acquire an excited level population which[37] does contribute through charge transfer to the populations of the Rydberg levels in impurity ions. This contribution can become dominant with tangential viewing near the plasma boundary radius where the recycling hydrogen has still an appreciable density $\sim 5 \times 10^9$ (H^0 atoms)/cm^3 (it can be an order g magnitude or more at the walls) and where the highly ionized, typically H- and He-like species, diffusing out from the core have not yet recombined. The radial viewing geometry, line-of-sight A, adopted for the absolute cross-section measurements in this study, serves to minimize l_r in Eq. (6) and therefore the contribution to the CX signal from excited background hydrogen atoms. The above considerations are very dependent on the O^{8+} transport to the outer plasma layers. Clearly, in the case where there is no CX signal prior to or succeeding the beam injection as in the O VIII signals, excited states in the recycled atomic hydrogen play no role. However, during beam injection the recycling rate of atomic hydrogen from the walls is likely to be increased and the solution of the problem depends on numerical models for the diffusion and transport of ionized impurities and of neutral hydrogen.

The presence of excited states in the beam itself is finally a problem to be considered. Lorentz fields induced by the motion of the beam across the toroidal field are sufficiently high to ensure the rapid depopulation of metastables via the s,p states to ground. At a field of 0.5 kV/cm the $2s,2p$ states of hydrogen have already about equal probability for decay, and for higher metastable levels the fields required are considerably lower.[38] External to the plasma, therefore, the beam population is negligible. In the plasma environment, however, excited-state populations of the atomic beams do exist as demonstrated by the appearance during the beam-injection period of Balmer emission with shifted wavelengths corresponding to the beam-energy fractions. The excited-state population can be estimated using a simple model in which collisional excitation by protons and electrons populates $n=2$ and depopulation occurs by radiative decay. The differential equation for the rates is

$$\frac{dn_2}{dt} = v_b \sigma_p n_1 n_p + \langle v_e \sigma_e \rangle n_1 n_e - A_{21} n_2 , \tag{7}$$

where v_b is the beam velocity. After setting $dn_2/dt = dn_2/dX v_b$ and considering $n_p = n_e$ equal to a constant and $\langle v_e \sigma_e \rangle$ also constant, the following solution obtains for the case in which the $n=1$ density remains approximately constant:

$$\frac{n_2(X)}{n_1} = \frac{v_b n_p}{A_{21}} \left[\sigma_p + \frac{\langle v_e \sigma_e \rangle}{v_b} \right] [1 - \exp(-A_{21} X / v_b)] . \tag{8}$$

We note that the characteristic length to achieve a steady-state excited population depends only on v_b and the transition probability of the $n=2$ states,

$$A_{21}/v_b=(4.78\times10^8)/(2.72\times10^8)=1.78\ \text{cm}^{-1}\ .$$

Therefore, the asymptotic steady-state population ratio is achieved by the time the beam particles penetrate only a very short distance into the plasma. Taking $\sigma_p=7\times10^{-17}$ cm^2 (40 keV), $\langle v_e\sigma_e\rangle=3.5\times10^{-8}$ cm^{3}s^{-1}, $v_b=2.72\times10^8$ cm s^{-1}, and $n_p=3\times10^{13}$ cm^{-3} gives

$$\frac{n_2}{n_1}=3.4\times10^{-3}\ .$$

Assuming the scaling (above) of $(n^*)^7$, we must conclude for the 40-keV component that approximately 40% of the $n=10$ excitation of O^{7+} arises from the $n=2$ population in the beam. The lower energy beam components have somewhat smaller fractions of $n=2$, and the fraction also depends on the plasma density. It does not seem, in conclusion, that charge exchange from the excited levels of the beam atoms can be completely neglected compared to excitation from the ground state. The excited-state corrections involved in this series of experiments, however, are of the same order as the errors involved in the data reduction.

ACKNOWLEDGMENTS

The authors are indebted to many individuals, to the ASDEX team, and to Euratom system of mobility contracts for the execution of this work. H. P. Summers and J. Spence of Strathclyde University have assisted with model calculations of the level populations. R. E. Olson (SRI International, Menlo Park, California) and W. Fritsch (Hahn Meitner Institute, Berlin) have freely provided the theoretical data on CX cross sections for the ASDEX beam energies. The encouragement and enthusiasm of W. Engelhardt and M. Von Hellerman (JET) have been much appreciated.

*Also at Clarendon Laboratory, University of Oxford, Oxford, England.

†Also at Royal Holloway College, University of London, London, England.

[1]R. C. Isler, Phys. Rev. Lett. **38**, 1359 (1977).

[2]V. V. Afrosimov, Yu S. Gorde'ev, A. N. Zinoviev, and A. A. Korotov, Fiz. Plazmy **5**, 987 (1979) [Sov. Plasma. Phys. **5**, 551 (1979)].

[3]R. J. Fonck, M. Finkenthal, R. J. Goldston, D. L. Herndon, R. A. Hulse, R. Kaita, and D. D. Meyerhofer, Phys. Rev. Lett. **49**, 737 (1982).

[4]R. C. Isler, L. E. Muray, S. Kasai, J. L. Dunlap, S. C. Bates, P. H. Edmonds, E. A. Lazarus, C. H. Ma, and M. Murakami, Phys. Rev. A **24**, 2701 (1981).

[5]R. C. Isler and R. A. Langley, Appl. Opt. **24**, 254 (1985).

[6]M. Keilhacker *et al., Tenth International Conference on Plasma Physics and Controlled Nuclear Fusion Research, London, September, 1984* (International Atomic Energy Agency, Vienna, 1985), Vol. I, pp. 71–85.

[7]E. J. Shipsey, T. A. Green, and J. C. Browne, Phys. Rev. A **27**, 821 (1983).

[8]W. Fritsch and C. D. Lin, Phys. Rev. A **49**, 3039 (1984).

[9]B. P. Duval, S. J. Fielding, N. C. Hawkes, J. Hugill, and N. J. Peacock, *Proceedings of the Twelth European Conference on Controlled Fusion and Plasma Physics, Budapest, 1985, Contributed Papers,* edited by L. Pócs and A. Montvai (European Physical Society, 1985), Vol. 9F, Part 1, pp. 203–206.

[10]S. Suckewer, C. H. Skinner, B. Stratton, R. Bell, A. Cavallo, J. Hosea, D. Dwang, and G. Schilling, Appl. Phys. Lett. **45**, 238 (1984).

[11]R. J. Fonck, R. J. Goldston, R. Kaita, R. and D. E. Post, Appl. Phys. Lett. **42**, 239 (1983).

[12]R. J. Groebner, N. H. Brooks, K. H. Burrell, and L. Rother, Appl. Phys. Lett. **43**, 920 (1983).

[13]R. C. Isler and L. E. Murray, Appl. Phys. Lett. **42**, 355 (1983).

[14]N. C. Hawkes and N. J. Peacock, Nucl. Fusion **25**, 971 (1985).

[15]R. J. Fonck, D. S. Darrow, and K. P. Jaehnig, Phys. Rev. A **29**, 3288 (1984).

[16]R. K. Janev, Phys. Scr. **T3**, 208 (1983).

[17]G. Fussmann *et al., Proceedings of the Twelth European Conference on Controlled Fusion and Plasma Physics, Budapest, 1985, Contributed Papers,* edited by L. Pócs and A. Montvai (European Physical Society, 1985), Vol. 9F, Part 1, pp. 195–198.

[18]R. J. Fonck, A. T. Ramsey, and R. V. Yelle, Appl. Opt. **21**, 2115 (1982).

[19]S. J. Fielding and D. Stork, Nucl. Fusion **22**, 617 (1982).

[20]T. A. Green, E. J. Shipsey, and J. C. Browne, Phys. Rev. A **25**, 1364 (1982).

[21]L. C. Green, P. P. Rush, and C. D. Chandler, Astrophys. J. Suppl. Ser. **3**, No. 37 (1957).

[22]D. H. Sampson, J. Phys. B **10**, 749 (1979).

[23]H. P. Summers (private communication).

[24]J. Spence and H. P. Summers, J. Phys. B **19**, 3749 (1986).

[25]B. P. Duval, Ph.D. thesis, University of Oxford, 1986.

[26]S. F. Gull and G. J. Daniell, Nature **272**, 686 (1978).

[27]K. H. Behringer, W. Engelhardt, and G. Fussmann, Proceedings of the International Atomic Energy Agency Technical Committee Meeting on Divertors and Impurity Control, [IPP Garching Report No. 42 1981 (unpublished)].

[28]K. H. Behringer, *et al.* JET Report No. JETP(85)08, 1985 (unpublished).

[29]G. Fussmann and J. Hofmann (unpublished).

[30]P. D. Morgan, K. H. Behringer, P. G. Carolan, M. J. Forrest, N. J. Peacock, and M. F. Stamp, Rev. Sci. Instrum. **56**, 962 (1985).

[31]P. G. Carolan, B. P. Duval, A. R. Field, S. J. Fielding, N. C. Hawkes, N. J. Peacock, G. Fussman, G. Janeschitz, F. Söldner, and K. H. Behringer, in *Proceedings of the Twelfth European Conference on Controlled Fusion, Budapest, 1985* (European Physical Society, 1985), Vol. 9F, Part 1, pp. 267–270.

[32]W. Fritsch (private communication).

[33]H. Ryufuku, Japan Atomic Energy Research Institute Report No. JAERI-82-031, 1982 (unpublished).

[34]R. E. Olson (private communication).

[35]M. G. V. Von Hellerman, W. W. Engelhardt, L. D. Horton, P.

G. Carolan, M. J. Forrest, and N. J. Peacock, in *Proceedings of the European Thirteenth Conference on Controlled Fusion and Plasma Physics, Schliesee, West Germany, 1986,* edited by G. B. Fardand, M. Kacfmann (European Physical Society, 1986), Vol. 10C, Part 2, pp. 120—123.

[36]R. K. Janev, B. Hl. Bransden, and J. W. Gallagher, J. Phys. Chem. Ref. Data **12**, 829 (1983).

[37]J. E. Rice, E. S. Marmar, J. L. Terry, E. Kallne, and J. Kallne, Phys. Rev. Lett. **56**, 50 (1986).

[38]J. le Normand, J. Phys. (Paris) **37**, 699 (1976).